

Reconstruction of phase dynamics from macroscopic observations based on linear and nonlinear response theories

Yoshiyuki Y. Yamaguchi ^{1,*} and Yu Terada ^{2,3,4,†}

¹Graduate School of Informatics, Kyoto University, Kyoto 606-8501, Japan

²Department of Neurobiology, University of California San Diego, La Jolla, California 92093, USA

³Institute for Physics of Intelligence, Department of Physics, Graduate School of Science, The University of Tokyo, 7-3-1 Hongo, Bunkyo-ku, Tokyo 113-0033, Japan

⁴Laboratory for Neural Computation and Adaptation, RIKEN Center for Brain Science, 2-1 Hirosawa, Wako, Saitama 351-0198, Japan



(Received 6 January 2023; revised 9 January 2024; accepted 22 January 2024; published 23 February 2024)

We propose a method to reconstruct the phase dynamics in rhythmical interacting systems from macroscopic responses to weak inputs by developing linear and nonlinear response theories, which predict the responses in a given system. By solving an inverse problem, the method infers an unknown system: the natural frequency distribution, the coupling function, and the time delay which is inevitable in real systems. In contrast to previous methods, our method requires neither strong invasiveness nor microscopic observations. We demonstrate that the method reconstructs two phase systems from observed responses accurately. The qualitative methodological advantages demonstrated by our quantitative numerical examinations suggest its broad applicability in various fields, including brain systems, which are often observed through macroscopic signals such as electroencephalograms and functional magnetic response imaging.

DOI: [10.1103/PhysRevE.109.024217](https://doi.org/10.1103/PhysRevE.109.024217)

I. INTRODUCTION

Rhythmical phenomena have been observed ubiquitously in nature as well as in engineering systems and attracted a wide spectrum of interests [1–3]. Specific rhythmical dynamics have been reported to play crucial functional roles in information processing in the brain [4,5]. Theoretical analysis has contributed to understanding the nature of interacting rhythmical systems. A highly beneficial tool is provided by the framework of phase reduction, which reduces a high-dimensional rhythmic dynamical system to a one-dimensional phase-oscillator system by eliminating the other nonessential degrees of freedom [6–8]. In this framework, a collective system of interacting units can be described by a coupled phase-oscillator system, which consists of the natural frequency distribution, coupling function, and time delay in interactions. A dynamical system behind an observed rhythmic phenomenon in the real world is mostly, however, unknown; the identification of the phase dynamics may help to understand the mechanism, predict the dynamics, and control the system [9]. It is thus in high demand to specify the underlying dynamical equations of coupled phase oscillators from accessible data.

While the inference problem has been extensively studied in coupled phase-oscillator systems [10–19] as well as other dynamical systems [20–23], there are still two crucial problems inseparable from their methods: The first is the assumption of accessibility to time series in almost all

individual elements. This assumption often cannot be satisfied in large complex systems: for example, in experiments of brain systems with electroencephalograms or functional magnetic response imaging (fMRI) signals, we record mesoscopic or macroscopic activity of neuronal populations and do not have full access to their microscopic details. The second is the neglect of the time delay. The existence of the delay is in principle inevitable in real systems, and can drastically change dynamics, for example, the stability of the nonsynchronized state [24,25]. It is a next step to develop a method that can be implemented with unknown delay in interactions.

Here, we utilize the linear response theory to infer coupled phase-oscillator systems [26–28] with the aid of a nonlinear response theory. We apply weak and oscillating external forces into a system, observe asymptotic responses of order parameters (macroscopic variables) with varying frequency of the external force, and infer the underlying phase dynamics by solving an inverse problem. Further, applied external forces are assumed substantially weak, since we focus on a regime where the linear response theory is valid. The weakness implies another advantage of noninvasiveness: the weak input prevents undesirable changes of the system [29,30]. We remark that our main target is the coupled phase-oscillator systems as previous works [10–19], and applicability of our method to an experimental system will be discussed lastly.

The assumptions on models here are that the system has mean-field, all-to-all homogeneous interactions and that the system lies in the nonsynchronized state, which is defined as the state with vanishing order parameters without an input in the limit of large system size. For the first assumption, it is worth remarking that the mean-field interaction is not extremely special, because the mean-field analysis is allowed

*yyama@amp.i.kyoto-u.ac.jp

†yuterada@ucsd.edu

in many other networks: small-world networks [31–33], scale-free networks [34], random networks [35], and oscillators on the one-dimensional lattice whose interaction strength decays algebraically with distance [36]. See also [37–39]. In addition, fMRI data suggest in functional connectivity a network structure with long-range interactions [40], which imply the potential approximate closeness to the mean-field class. As for the second assumption, experimental observations suggest that nonsynchronized states in neural activity are associated with cognitive functions [41,42], and therefore it is an important issue to study nonsynchronized states. Moreover, inferred results in the nonsynchronized state apart from the coupling strengths are carried over to partially synchronized states even after a spontaneous synchronization emerges. We remark that a repetition of observation is reasonably practical for different external frequencies, since the system returns to the nonsynchronized state exponentially fast after cutting off the external force [43].

This paper is organized as follows. The coupled phase-oscillator model and the linear susceptibility are introduced in Sec. II. The inference theory proposed in this paper is reported in Sec. III with a nonlinear susceptibility. The theory is examined in two models in Sec. IV. Section V is devoted to a summary and discussions.

II. SUSCEPTIBILITY IN COUPLED PHASE OSCILLATORS

Based on the phase reduction [44], we consider mean-field coupled oscillators governed by the phase equation

$$\frac{d\theta_j}{dt} = \omega_j + \frac{1}{N} \sum_{k=1}^N \Gamma[\theta_j(t) - \theta_k(t - \tau)] + H(\theta_j(t), t; \omega_{\text{ex}}). \quad (1)$$

See Appendix A for a derivation and assumptions. The variable $\theta_j(t)$ represents the phase of the j th oscillator at time t , the constant ω_j is the natural frequency that follows the natural frequency distribution $g(\omega)$, the function Γ represents the coupling function, and the constant τ is the time delay for the couplings. The function H represents the external force and the constant ω_{ex} is its frequency. The 2π -periodic functions Γ and H are expanded into the Fourier series as

$$\Gamma(\theta) = - \sum_{m=1}^{\infty} K_m \sin(m\theta + \alpha_m) \quad (2)$$

and

$$H(\theta, t; \omega_{\text{ex}}) = -\Theta(t) \sum_{m=1}^{\infty} h_m \sin[m(\theta - \omega_{\text{ex}}t)], \quad (3)$$

where h_m is nonnegative strength and $\Theta(t)$ is the unit step function. We neglect the zero mode $m = 0$ in Γ since the constant can be included in ω_j , and in H since there is no corresponding linear response in the order parameters [45] [see (B10)]

$$z_n(t) = \frac{1}{N} \sum_{k=1}^N e^{in\theta_k(t)}. \quad (4)$$

The intrinsically determined but unknown objects in (1) are $g(\omega)$, $\Gamma(\theta)$ (namely $\{K_m, \alpha_m\}$), and τ , while the controllable

parameters are ω_{ex} and

$$\mathbf{h} = (h_1, h_2, \dots). \quad (5)$$

We will infer the unknown objects from asymptotic responses of the order parameters (4) with varying the external frequency ω_{ex} and fixing \mathbf{h} . We assume that all elements of \mathbf{h} are sufficiently small. This assumption ensures highly weak invasiveness of our method.

The inference theory developed in Sec. III is based on the assumptions that we can apply the above external force \mathbf{h} arbitrarily and that we can observe corresponding responses in z_n . Due to these assumptions, applicability of the theory to experimental data is not obvious and will be discussed in Sec. V. Nevertheless, we underline that a benefit of our inference theory is its universality founded on the phase reduction.

The asymptotic response is written up to $O(\|\mathbf{h}\|^2)$ as

$$e^{-in\omega_{\text{ex}}t} z_n(t) \xrightarrow{t \rightarrow \infty} \chi_n(\omega_{\text{ex}}) h_n + \sum_{l,m} \chi_n^{lm}(\omega_{\text{ex}}) h_l h_m. \quad (6)$$

Taking the limit $N \rightarrow \infty$ [46], the linear response coefficient, susceptibility $\chi_n(\omega_{\text{ex}})$ is obtained as [28]

$$\chi_n(\omega_{\text{ex}}) = \frac{\mathcal{G}(\omega_{\text{ex}})}{2 - L_n(\omega_{\text{ex}})\mathcal{G}(\omega_{\text{ex}})} \quad (n > 0), \quad (7)$$

where

$$L_n(\omega_{\text{ex}}) = K_n e^{-i(\alpha_n + n\omega_{\text{ex}}\tau)}, \quad (8)$$

$$\mathcal{G}(\omega_{\text{ex}}) = \pi g(\omega_{\text{ex}}) + i \text{P.V.} \int_{-\infty}^{\infty} d\omega \frac{g(\omega)}{\omega - \omega_{\text{ex}}}, \quad (9)$$

and the symbol P.V., indicates the Cauchy principal value. The left-hand side of (7) corresponds to observed data while the right-hand side consists of the unknown objects. While the derivation of (7) for a given system is a forward problem, we address here the inverse problem to infer the unknown objects.

III. INFERENCE THEORY

We underline that the inference using (7) is not straightforward. For a fixed ω_{ex} and a mode n , the left-hand side contains one known complex value (χ_n), while the right-hand side contains two unknown complex values (\mathcal{G} and L_n). To overcome this difficulty, we introduce two ideas. The first one is orthogonality of $\{e^{-in\omega_{\text{ex}}\tau}\}$, which permits us to infer all the unknown objects, if the time delay is not zero, $\tau \neq 0$. The second one is the incorporation of a nonlinear susceptibility, which covers the case $\tau = 0$. Here we use a nonlinear response:

$$\chi_2^{11}(\omega_{\text{ex}}) = \frac{2i\mathcal{G}'(\omega_{\text{ex}})}{[2 - L_2(\omega_{\text{ex}})\mathcal{G}(\omega_{\text{ex}})][2 - L_1(\omega_{\text{ex}})\mathcal{G}(\omega_{\text{ex}})]^2}. \quad (10)$$

See Appendix B for a derivation. We note that, once we infer one L_m , say L_n , the other ones are inferred through the relation

$$L_m(\omega_{\text{ex}}) = L_n(\omega_{\text{ex}}) + \frac{1}{\chi_n(\omega_{\text{ex}})} - \frac{1}{\chi_m(\omega_{\text{ex}})}. \quad (11)$$

With an inferred $L_m(\omega_{\text{ex}})$, $g(\omega)$ is also inferred by

$$g(\omega) = \frac{1}{\pi} \text{Re} \mathcal{G}(\omega) = \frac{1}{\pi} \text{Re} \left[\frac{2\chi_m(\omega)}{1 + L_m(\omega)\chi_m(\omega)} \right]. \quad (12)$$

Therefore, the key task is to infer one L_m .

Our method is twofold: inference of τ (procedure 1) and of $K_m e^{-i\alpha_m}$ (procedure 2). The latter is further decomposed into the two cases of $\tau \neq 0$ (procedure 2A) and $\tau = 0$ (procedure 2B).

Before going into details, we define the reliable sampling. We observe $\chi_n(\omega_{\text{ex}})$ and $\chi_1^{22}(\omega_{\text{ex}})$ for a set of external frequency $\Omega^S = \{\omega_{\text{ex}}^1, \dots, \omega_{\text{ex}}^S\}$ ($\omega_{\text{ex}}^1 < \dots < \omega_{\text{ex}}^S$). We call a sampling set Ω^S reliable, when the range $\omega_{\text{ex}}^S - \omega_{\text{ex}}^1$ is sufficiently large and the gaps $\omega_{\text{ex}}^{i+1} - \omega_{\text{ex}}^i$ are sufficiently small.

Procedure 1 performs a finite Fourier transform:

$$L_{mn}(t) = \frac{1}{\omega_{\text{ex}}^S - \omega_{\text{ex}}^1} \int_{\omega_{\text{ex}}^1}^{\omega_{\text{ex}}^S} \left[\frac{1}{\chi_n(\omega_{\text{ex}})} - \frac{1}{\chi_m(\omega_{\text{ex}})} \right] e^{i\omega_{\text{ex}} t} d\omega_{\text{ex}}. \quad (13)$$

Looking back at the relation (11) and the definition of L_m , the absolute value $|L_{mn}(t)|$ has two peaks ($\tau \neq 0$) or one peak ($\tau = 0$) at $t = m\tau$ and $n\tau$ because of the orthogonality of $\{e^{-in\omega_{\text{ex}} t}\}$, if the sampling set is reliable. The peak positions infer the time delay τ . We give two remarks. First, in an actual sampling, discreteness and finiteness of the sampling set Ω^S cause errors of the orthogonality. Second, since $L_{mn}(m\tau) = K_m e^{-i\alpha_m}$, the errors should be sufficiently small to observe a clear peak of the height K_m at $t = m\tau$.

Procedure 2A directly uses $L_{mn}(m\tau) = K_m e^{-i\alpha_m}$ for any m , and the factor $L_m(\omega)$ is obtained with τ inferred in procedure 1. The natural frequency distribution $g(\omega)$ is inferred for each m from (12). We solely used linear responses up to this procedure.

Procedure 2B is for $\tau = 0$, since the peak at $t = 0$ mixes the modes m and n , $L_{mn}(0) = K_m e^{-i\alpha_m} - K_n e^{-i\alpha_n}$. To decompose the mixture, we use the nonlinear response (10). z_2 in $O(\|\mathbf{h}\|^2)$ can be directly observed by applying the external force in the first mode $\mathbf{h} = (h_1, 0, 0, \dots)$, because $\chi_2(\omega_{\text{ex}}) \equiv 0$ in this setting. Solving (10) we have one expression of $\mathcal{G}'(\omega_{\text{ex}})$. We independently have another expression of $\mathcal{G}'(\omega_{\text{ex}})$ through solving (7) by \mathcal{G} and deriving it. The combination of the above two expressions of $\mathcal{G}'(\omega_{\text{ex}})$ gives

$$L_1 = K_1 e^{-i\alpha_1} = \frac{2\chi_2^{11}(\omega_{\text{ex}})}{i\chi_2(\omega_{\text{ex}})\chi_1'(\omega_{\text{ex}})} - \frac{1}{\chi_1(\omega_{\text{ex}})} \quad (14)$$

for $\tau = 0$ (see Appendix C1). We take the average over S estimated values of L_1 from $\omega_{\text{ex}}^1, \dots, \omega_{\text{ex}}^S$. The other coefficients L_m ($m > 1$) are estimated from (11) by taking the average. We remark that procedure 2B is also applicable for $\tau > 0$, where L_1 is obtained as a solution to a quadratic equation. However, procedure 2A provides higher performance in inference for a nonzero time-delay case as compared in an application (see Appendix C2).

IV. NUMERICAL TESTS

By employing the theory developed above, we tackle a reconstruction problem in two models: model 1 has a delay, that is, $\tau > 0$ and procedure 2A is applied, while model 2

TABLE I. True and inferred parameter values of model 1 and model 2. The inferred values are given for each sampling set. NI means noninferred values, because there is no clear peak around $t = 3\tau$ in either $|L_{34}|$ or $|L_{35}|$. Procedure 1 implies that K_4 should be sufficiently small from absence of a clear peak of $|L_{45}(t)|$ [see Fig. 1(d)].

Model 1	τ	K_1	α_1	K_2	α_2	K_3	α_3
Truth	2	1.379	0.7884	0.568	-3.0316	0.154	-0.7546
Ω_1^{50}	1.987	1.383	0.820	0.596	-3.016	0.153	-0.864
Ω_1^{25}	1.995	1.381	0.793	0.582	-3.111	NI	NI
Model 2	τ	K_1	α_1	K_2	α_2		
Truth	0	1	1	0	0		
Ω_2^{81}	0.001	0.958	1.001	0.044	-2.119		
Ω_2^{41}	-0.001	1.063	0.497	0.521	-0.706		

does not and procedure 2B is in use. Their system parameters are arranged in Table I. Numerical simulations of (1) are performed in the use of the second-order Runge-Kutta algorithm with the time step $\Delta t = 0.01$. Responses of order parameters are obtained as the average in the time interval $t \in (50, 150]$. The number of oscillators is $N = 10^5$. All the numerical simulations are performed by activating only one mode in \mathbf{h} with strength 0.1: $h_m = 0.1$ and $h_n = 0$ ($n \neq m$) for the m th mode. This strength is sufficiently small for the linear response but sufficiently large for overcoming finite-size fluctuation of order $O(1/\sqrt{N})$ by the second-order response of order $O(\|\mathbf{h}\|^2)$.

Model 1 is motivated by neurobiological systems and is connected directly to a network of the Hodgkin-Huxley neurons. As in [47,48], the Fourier components of the modes m ($m \geq 4$) are zero. The time delay is set as $\tau = 2$, which is compatible with experimental observations [49]. Taking another experimental observation [50] into account, we assume the log-normal natural frequency distribution:

$$g_1(\omega) = \frac{1}{\omega \sqrt{2\pi\sigma_1^2}} \exp \left[-\frac{(\ln \omega - \mu_1)^2}{2\sigma_1^2} \right] \quad (15)$$

with $\mu_1 = \ln 5$ and $\sigma_1 = 1$. The external frequency is sampled from the interval $\omega_{\text{ex}} \in [0.2, 10]$ with the step $\Delta\omega_{\text{ex}} = 0.2$ for the sampling set Ω_1^{50} , and $\Delta\omega_{\text{ex}} = 0.4$ for the set Ω_1^{25} . We start from procedure 1. We approximately compute $L_{mn}(t)$ (13) by using the midpoint algorithm, where a sampling point ω_{ex}^i is the midpoint. Absolute values $|L_{mn}(t)|$ for the set Ω_1^{50} are reported in Fig. 1. We obtain the estimate $\tau = 1.987$ by taking the average over the largest peak positions for the pairs $(m, n) = (3, 4)$ and (m', n') ($m' = 1, 2; n' = m' + 1, \dots, 5$). A graph should have two large peaks at $t = m\tau$ and $n\tau$, although some peaks are not visible in Fig. 1. No clear peak at $t = n\tau$ implies that K_n is smaller than the error level. Indeed, no clear peak of $|L_{45}(t)|$ in Fig. 1(d) is consistent with $K_4 = K_5 = 0$. Procedure 2A infers the coefficients L_m are from the value of $L_{mn}(t)$ at the peak position, where the above mentioned pairs are in use to take the average. Performing the same procedure but using the set Ω_1^{25} , we obtain another set of inferences. The inferences are compared with the true values in Table I. The coupling function $\Gamma_1(\theta)$ is directly obtained from L_m , and the natural frequency distribution $g_1(\omega)$ is

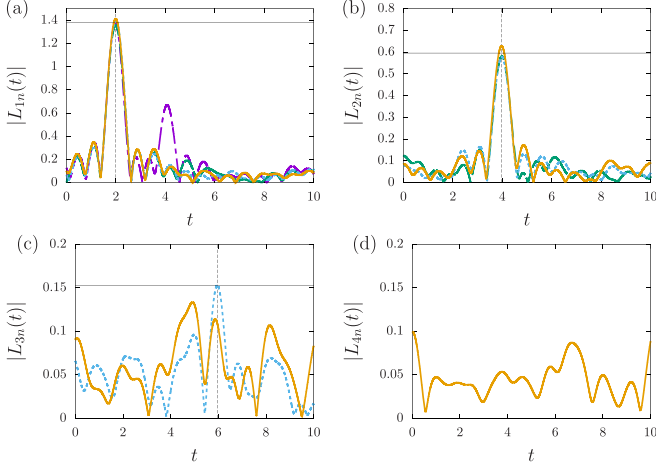


FIG. 1. Procedure 1 in model 1. $|L_{mn}(t)|$ (13) is computed from the sampling set Ω_1^{50} . (a) $m = 1$ and $n \in \{2, 3, 4, 5\}$. (b) $m = 2$ and $n \in \{3, 4, 5\}$. (c) $m = 3$ and $n \in \{4, 5\}$. (d) $m = 4$ and $n \in \{5\}$. The lines are $n = 2$ (purple chain), $n = 3$ (green broken), $n = 4$ (blue dotted), and $n = 5$ (orange solid). The vertical dashed black lines mark the inferred time delay $m\tau$, and the horizontal solid black lines mark the inferred K_m .

inferred through the relation (12). They are in good agreement with the true ones for the set Ω_1^{50} as exhibited in Fig. 2. Increasing the number of samples improves the inference, because the sampling set becomes more reliable.

Model 2 is the Sakaguchi-Kuramoto model [51] which is specified by the parameter set $(K_1, \alpha_1) = (1, 1)$ and the other Fourier modes are zero. The time delay is zero: $\tau = 0$. To demonstrate the ability of the proposed method for general natural frequency distributions, a nonunimodal and asymmetric natural frequency distribution is assumed as

$$g_2(\omega) = \frac{ae^{-(x-\mu_2)^2/(2\sigma_2^2)} + (1-a)e^{-(x+\mu_2)^2/(2\sigma_2^2)}}{\sqrt{2\pi\sigma_2^2}}, \quad (16)$$

where $a = 0.8$, $\mu_2 = 2$, and $\sigma_2 = 1$. The external frequency is sampled from $\omega_{\text{ex}} \in [-4, 4]$ with the step $\Delta\omega_{\text{ex}} = 0.1$ for the sampling set Ω_2^{81} and $\Delta\omega_{\text{ex}} = 0.2$ for the set Ω_2^{41} . To compute the derivative $\chi'_1(\omega_{\text{ex}})$, we use the central difference except for the head and the end points, namely ω_{ex}^1 and ω_{ex}^S ,

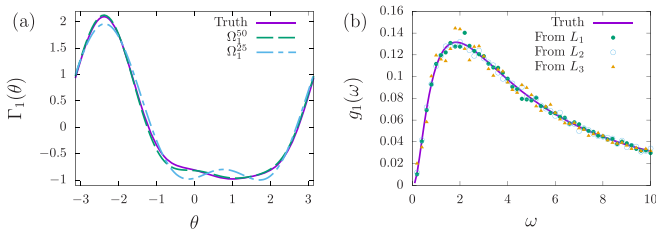


FIG. 2. Comparison between the truth (purple solid line) and the inference in model 1 having $\tau > 0$. (a) The coupling function is $\Gamma_1(\theta)$. The sampling sets are Ω_1^{50} (green broken line) and Ω_1^{25} (blue chain line). (b) The natural frequency distribution $g_1(\omega)$ (15) is obtained from the inferred L_1 (green filled circles), L_2 (blue open circles), and L_3 (orange triangles) by (12). The sampling set is Ω_1^{50} .

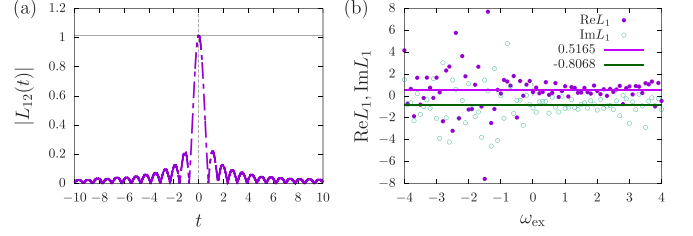


FIG. 3. Model 2. (a) Procedure 1. The peak position is $\tau = 0.001$ and the peak height is 1.014. (b) Procedure 2B is used to infer L_1 by (14) for each external frequency ω_{ex} . The real part $\text{Re}L_m$ (purple filled circles) and the imaginary part $\text{Im}L_m$ (green open circles) are shown. The purple and green horizontal solid lines mark the averaged values. The sampling set is Ω_2^{81} .

for which the forward and backward differences are in use, respectively.

From now on, we concentrate on inferences of L_1 and L_2 . Procedure 1 confirms that $|L_{12}(t)|$ has a large peak at $t = 0.001$ [see Fig. 3(a)], and hence we conclude no time delay, $\tau = 0$. The peak height 1.014 corresponds to $|K_1 e^{-i\alpha_1} - K_2 e^{-i\alpha_2}|$, and the fact $K_2 = 0$ implies that the peak height approximately infers the value of $K_1 = 1$. However, we do not know the value of K_2 a priori, and we cannot determine K_1 yet. We thus use procedure 2B, (14), for inferring L_1 , and (11) for L_2 . They are obtained as functions of ω_{ex} , and $L_1(\omega_{\text{ex}})$ is reported in Fig. 3(b). Fluctuation of L_1 may be reasonable, because procedure 2B, (14), uses a derivative χ'_1 and a nonlinear susceptibility χ_2^{11} , while procedure 2A uses only the linear susceptibilities χ_n . We determine the inferred values of the constants L_1 and L_2 by taking the average over ω_{ex} , and the constants K_m and α_m ($m = 1, 2$) from the averaged L_m . The inferred values are arranged in Table I. The set Ω_2^{81} infers good values, while the set Ω_2^{41} does not provide good inferences, owing to the lack of precision in computation of the derivative $\chi'_1(\omega_{\text{ex}})$. The inferred coupling function Γ_2 and the natural frequency distribution $g_2(\omega)$ agree with the true ones as reported in Fig. 4.

V. SUMMARY AND DISCUSSIONS

In summary, we proposed a method to reconstruct the underlying coupled phase-oscillator model of a collective

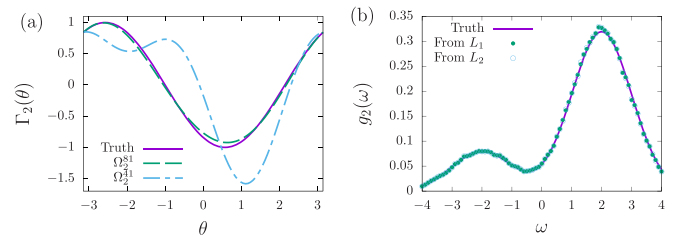


FIG. 4. Comparison between the truth (purple solid line) and the inference in model 2 having $\tau = 0$. (a) The coupling function is $\Gamma_2(\theta)$. The sampling sets are Ω_2^{81} (green broken line) and Ω_2^{41} (blue chain line). (b) The natural frequency distribution $g_2(\omega)$ (16) is obtained from the inferred L_1 (green filled circles) and L_2 (blue open circles) through (12). The sampling set is Ω_2^{81} .

rhythmic system by observing responses in order parameters to weak external forces with varying the frequency. A significant advantage of the proposed method is that it requires neither severe invasiveness nor microscopic observations of individual elements. The effectiveness is confirmed successfully by applying it to two representative phase models, where the unknown objects including the time delay in interactions have been inferred accurately, when the sampling of the external frequency lies on a sufficiently large range with sufficiently small gaps. We note that the proposed method has a potential to understand the criticality in complex systems in terms of synchronization transitions, which may reveal another perspective of the brain systems such as their computational benefits [52]. Recently, experimental observation techniques on mesoscopic neuronal activity have been advanced rapidly, which may provide crucial insights on whole-brain mechanisms of neural computation beyond technical limitation of microscopic observation [53]. Our method is expected to bridge the gap between such data and theoretical analysis. To apply our method to biological data, it is important to study how raw or processed mesoscopic or macroscopic data (for example [54]) are related to order parameters used here. It would be useful to export the idea of our theory to synchronized states, noisy systems, complex networks, and other dynamical systems [20–23,55].

Finally, we discuss three difficulties to apply the proposed method to experimental data. The first difficulty is the complexity of susceptibilities $\chi_n(\omega_{\text{ex}})$. These susceptibilities can be obtained from the Daido-Kuramoto order parameters (4). A methodology to connect experimentally observed quantities and these order parameters should be sought. The second difficulty is the restriction of observables. In the two-dimensional FitzHugh-Nagumo model, for example, the membrane potential v is observable and the other variable may not be. The third difficulty is the restriction of the external force H . Indeed, in coupled phase oscillators, the Fourier modes of the external force are determined by the phase sensitivity function $\mathbf{Z}(\theta)$ of the limit cycle oscillator (see Appendix A for details). In other words, we cannot choose the external force vector $\mathbf{h} = (h_1, h_2, \dots)$ arbitrarily. We give a scenario to overcome the above difficulties. First, the complexity of susceptibilities is not essential, since the Kramers-Kronig relation reproduces the imaginary part from the real part. Second, moments of an observable variable, assumed to be observable, provide a set of conditions which susceptibilities must satisfy. The third difficulty is rather essential, since a Fourier mode of the coupling function $\Gamma(\theta)$ is not accessible in the linear level if the external force H does not have the Fourier mode. However, a nonlinear response helps to reveal a forbidden Fourier mode of $\Gamma(\theta)$ as the susceptibility χ_2^{11} provides information on the second Fourier mode of Γ from the first Fourier mode of H . We have to examine feasibility and precision of the above scenario. We leave development of an inference theory for the higher-dimensional dynamics as a future subject.

ACKNOWLEDGMENTS

Y.Y.Y. acknowledges the support of Japan Society for the Promotion of Science (JSPS) KAKENHI Grants No. JP16K05472 and No. JP21K03402. Y.T. was supported by the

Special Postdoctoral Research Program at RIKEN and JSPS KAKENHI Grant No. JP19K20365.

APPENDIX A: PHASE REDUCTION

We consider a coupled high-dimensional dynamics

$$\frac{d\mathbf{x}_j}{dt} = \mathbf{F}_j(\mathbf{x}_j) + \epsilon \sum_{k=1}^N \mathbf{G}_{jk}(\mathbf{x}_j, \mathbf{x}_k) + \epsilon \mathbf{H}_j(t), \quad \mathbf{x}_j \in \mathbb{R}^d \quad (\text{A1})$$

which describes a realistic system. The dynamics \mathbf{F}_j may be the van der Pole system ($d = 2$), the FitzHugh-Nagumo system ($d = 2$), or the Hodgkin-Huxley model ($d = 4$). The last term $\mathbf{H}_j(t)$ represents the external force, which does not depend on θ_j to avoid observation of individual elements. The time delay in (1) is introduced phenomenologically, and we skip it here (see [56,57] for phase reductions of differential equations with a time delay).

We assume that $|\epsilon|$ is sufficiently small ($|\epsilon| \ll 1$) so that we can perform the phase reduction and consider the linear response. Further, \mathbf{F}_j , \mathbf{G}_{jk} , and \mathbf{H}_j are assumed to be expanded into

$$\mathbf{F}_j(\mathbf{x}_j) = \mathbf{F}(\mathbf{x}_j) + \epsilon \mathbf{f}_j(\mathbf{x}_j), \quad (\text{A2})$$

$$\mathbf{G}_{jk}(\mathbf{x}_j, \mathbf{x}_k) = \mathbf{G}(\mathbf{x}_j, \mathbf{x}_k) + \epsilon \mathbf{g}_{jk}(\mathbf{x}_j, \mathbf{x}_k), \quad (\text{A3})$$

and

$$\mathbf{H}_j(t) = \mathbf{H}(t) + \epsilon \mathbf{h}_j(t). \quad (\text{A4})$$

Let $\mathbf{U}(t)$ be the unique limit cycle solution with the period $2\pi/\omega$ to the dynamical system $\dot{\mathbf{x}} = \mathbf{F}(\mathbf{x})$. We introduce the phase function $\phi(\mathbf{x})$ in the basin of the limit cycle, which satisfies $\nabla\phi(\mathbf{x}) \cdot \mathbf{F}(\mathbf{x}) = \omega$ for any \mathbf{x} in the basin. The phase θ_j of the j th element \mathbf{x}_j is defined as $\theta_j = \phi(\mathbf{x}_j)$. Deriving the phase with respect to t , we have

$$\frac{d\theta_j}{dt} = \omega + \epsilon \nabla\phi(\mathbf{x}_j) \cdot \left[\mathbf{f}_j(\mathbf{x}_j) + \sum_{k=1}^N \mathbf{G}_{jk}(\mathbf{x}_j, \mathbf{x}_k) + \mathbf{H}_j(t) \right]. \quad (\text{A5})$$

Asymptotically, we may write an orbit as $\mathbf{x}_j = \mathbf{U}(t) + \epsilon \mathbf{u}_j(t)$, and it is sufficient to replace \mathbf{x}_j with \mathbf{U} to have a phase equation up to $O(\epsilon)$. Keeping in mind the phases of \mathbf{x}_j and \mathbf{x}_k differ in general, taking the average over a period of the limit cycle, we have the equation of θ_j as

$$\frac{d\theta_j}{dt} = \omega_j + \frac{1}{N} \sum_{k=1}^N \Gamma(\theta_j - \theta_k) + H(\theta_j, t), \quad (\text{A6})$$

where $\omega_j - \omega$, Γ , and H respectively come from $\mathbf{Z}(\theta_j) \cdot \mathbf{f}_j$, $\mathbf{Z}(\theta_j) \cdot \mathbf{G}$, and $\mathbf{Z}(\theta_j) \cdot \mathbf{H}$ on the limit cycle, and $\mathbf{Z}(\theta) = \nabla\phi[\mathbf{U}(\theta/\omega)]$ is the phase response function. Note that \mathbf{g}_{jk} , \mathbf{h}_j , and \mathbf{u}_j are absent in (A6).

APPENDIX B: LINEAR AND NONLINEAR RESPONSE THEORIES

The response theories are derived from the equation of continuity, which describes dynamics of phase oscillators in

the limit $N \rightarrow \infty$. The equation of continuity is introduced in Appendix B1, the linear response theory reported in [28] is reviewed in Appendix B2, and the nonlinear response theory is developed in Appendix B3.

1. Equation of continuity

Dynamics of the system (1) is described in the limit $N \rightarrow \infty$ by the equation of continuity

$$\frac{\partial F}{\partial t} + \frac{\partial}{\partial \theta} \{[\omega + v[F] + H(\theta, t; \omega_{\text{ex}})]F\} = 0, \quad (\text{B1})$$

where $F(\theta, \omega, t)d\theta d\omega$ represents the fraction of oscillators which are found in the small area $[\theta, \theta + d\theta] \times [\omega, \omega + d\omega]$ at time t , and

$$v[F](\theta, t; \tau) = \int_{-\infty}^{\infty} d\omega \int_0^{2\pi} d\theta' \Gamma(\theta - \theta') F(\theta', \omega, t - \tau). \quad (\text{B2})$$

Suppose that the nonsynchronized state

$$F_0(\omega) = \frac{g(\omega)}{2\pi} \quad (\text{B3})$$

is stable stationary under $H \equiv 0$. We expand F around F_0 as

$$F(\theta, \omega, t) = F_0(\omega) + f^{(1)}(\theta, \omega, t) + f^{(2)}(\theta, \omega, t) + \dots, \quad (\text{B4})$$

where $f^{(k)} = O(\|H\|^k)$. Substituting the expansion (B4) into the equation of continuity (B1), we have

$$\frac{\partial f^{(1)}}{\partial t} + \frac{\partial}{\partial \theta} [\omega f^{(1)} + (v[f^{(1)}] + H)F_0] = 0 \quad (\text{B5})$$

in the order of $O(\|H\|)$, and

$$\frac{\partial f^{(2)}}{\partial t} + \frac{\partial}{\partial \theta} \{\omega f^{(2)} + v[f^{(2)}]F_0 + (v[f^{(1)}] + H)f^{(1)}\} = 0 \quad (\text{B6})$$

in the order of $O(\|H\|^2)$. We introduce the k th order part of the order parameters as

$$z_n^{(k)}(t) = \int_{-\infty}^{\infty} d\omega \int_0^{2\pi} d\theta e^{in\theta} f^{(k)}(\theta, \omega, t). \quad (\text{B7})$$

From now on, we denote the Fourier series expansion of a function $\varphi(\theta, t)$ as

$$\varphi(\theta, t) = \sum_n e^{in\theta} \tilde{\varphi}_n(t), \quad (\text{B8})$$

and the Laplace transform of $\tilde{\varphi}_n(t)$ as

$$\hat{\varphi}(s) = \int_0^{\infty} e^{-st} \tilde{\varphi}_n(t) dt, \quad \text{Re}(s) > 0. \quad (\text{B9})$$

The domain $\text{Re}(s) > 0$ is introduced to ensure the convergence of the integral.

2. Linear response: $O(\|H\|)$

A derivation of the linear response has been reported in [28]. We review a necessary part in computations of $O(\|H\|^2)$. The Fourier-Laplace transform of $f^{(1)}$ satisfies

$$(s + in\omega) \hat{f}_n^{(1)} + in(\Gamma_n e^{-s\tau} \hat{z}_{-n}^{(1)} + \hat{H}_n) F_0 = 0. \quad (\text{B10})$$

Using the definition (B7), we have

$$\hat{z}_{-n}^{(1)}(s) = -\frac{\hat{H}_n(s; \omega_{\text{ex}})}{\Lambda_n(s)} I_n(s), \quad (\text{B11})$$

where

$$\Lambda_n(s) = 1 + \Gamma_n e^{-s\tau} I_n(s) \quad (\text{B12})$$

and

$$I_n(s) = \int_L \frac{g(\omega)}{\omega - is/n} d\omega. \quad (\text{B13})$$

In $I_n(s)$, the singular point $\omega = is/n$ moves from the upper or lower half of the complex ω plane with varying $\text{Re}(s)$ from $\text{Re}(s) > 0$ to $\text{Re}(s) \leq 0$. The integral contour L is modified continuously from the real axis to avoid the singular point $\omega = is/n$, and the modification induces a residue part [28]. The explicit form of $I_n(s)$ is

$$I_n(s) = \begin{cases} \int_{-\infty}^{\infty} \frac{g(\omega)}{\omega - is/n} d\omega & (\text{Re}(s) > 0) \\ \text{P.V.} \int_{-\infty}^{\infty} \frac{g(\omega)}{\omega - is/n} d\omega + \frac{n}{|n|} i\pi g(is/n) & (\text{Re}(s) = 0) \\ \int_{-\infty}^{\infty} \frac{g(\omega)}{\omega - is/n} d\omega + \frac{n}{|n|} i2\pi g(is/n) & (\text{Re}(s) < 0) \end{cases} \quad (\text{B14})$$

where P.V. represents the Cauchy principal value.

The linear susceptibility (7) is obtained by picking up the pole of $\hat{H}_n(s; \omega_{\text{ex}})$, which survives in $t \rightarrow \infty$. A notable feature is that no response appears in z_n for an external force of a different mode \hat{H}_m ($|m| \neq |n|$).

3. Nonlinear response: $O(\|H\|^2)$

The Fourier-Laplace transform of $f^{(2)}$ satisfies

$$(s + in\omega) \hat{f}_n^{(2)} + in(\Gamma_n e^{-s\tau} \hat{z}_{-n}^{(2)} F_0 + \hat{N}_n^{(2)}) = 0, \quad (\text{B15})$$

where

$$N_n^{(2)}(\omega, t) = \sum_m V_m(t) f_{n-m}^{(1)}(\omega, t) \quad (\text{B16})$$

and

$$V_m(t) = \Gamma_m z_{-m}^{(1)}(t - \tau) + H_m(t). \quad (\text{B17})$$

The Laplace transform of $z_{-n}^{(2)}(t)$ is obtained as

$$\hat{z}_{-n}^{(2)}(s) = \frac{-2\pi}{\Lambda_n(s)} \int_{-\infty}^{\infty} \frac{\hat{N}_n^{(2)}(\omega, s)}{\omega - is/n} d\omega. \quad (\text{B18})$$

We need the Laplace transform of $N_n^{(2)}$, which consists of products of two functions.

a. Laplace transform of a product function

For analytic functions $f(t)$ and $g(t)$, we have the relation

$$\hat{f}g(s) = \frac{1}{2\pi i} \int_{\sigma_g - i\infty}^{\sigma_g + i\infty} \hat{f}(s - s') \hat{g}(s') ds', \quad (\text{B19})$$

where $\sigma_g \in \mathbb{R}$ is larger than the real parts of any singularities of $\hat{g}(s)$. A proof of (B19) is straightforward. We denote the inverse Laplace transforms of $\hat{f}(s)$ and $\hat{g}(s)$ as

$$f(t) = \frac{1}{2\pi i} \int_{\sigma_f - i\infty}^{\sigma_f + i\infty} e^{st} \hat{f}(s) ds, \quad (\text{B20})$$

where $\sigma_f \in \mathbb{R}$ is larger than the real parts of any singularities of $\tilde{f}(s)$, and

$$g(t) = \frac{1}{2\pi i} \int_{\sigma_g - i\infty}^{\sigma_g + i\infty} e^{s_2 t} \tilde{g}(s_2) ds_2. \quad (\text{B21})$$

Changing the variables as $(s, s') = (s_1 + s_2, s_2)$, the product function $(fg)(t)$ is expressed as

$$(fg)(t) = \frac{1}{2\pi i} \int_{\sigma_f + \sigma_g - i\infty}^{\sigma_f + \sigma_g + i\infty} ds e^{st} \times \left[\frac{1}{2\pi i} \int_{\sigma_g - i\infty}^{\sigma_g + i\infty} ds' \tilde{f}(s - s') \tilde{g}(s') \right]. \quad (\text{B22})$$

The integral over s is the inverse Laplace transform of the inside of the square brackets, and hence we have the relation (B19).

We note that we pick up the singularities of \tilde{g} only in the integral with respect to s' . Let a be a pole of $\tilde{f}(s)$, and let b be a pole of $\tilde{g}(s)$. By the definitions, we have $\text{Re}(a) < \sigma_1$ and $\text{Re}(b) < \sigma_2$. The convolution yields a pole of \tilde{f} which lies on the right side of the line $\text{Re}(s') = \sigma_g$, since $s' = s - a = \sigma_f + \sigma_g - a > \sigma_g$. Therefore, this singularity is not enclosed by the integral counter, which consists of the line $\text{Re}(s') = \sigma_g$ and the left half circle passing through the point at infinity on the left half complex s' plane.

b. Convolution in $\hat{N}_n^{(2)}$

In this subsection we omit ω_{ex} in H_m for simplicity of notation. The Laplace transform $\hat{z}_{-n}^{(2)}(s)$ is expressed as

$$\hat{z}_{-n}^{(2)}(s) = \frac{-2\pi}{\Lambda_n(s)} \sum_m \int_{-\infty}^{\infty} \frac{\mathcal{L}[V_m f_{n-m}^{(1)}](s)}{\omega - is/n} d\omega, \quad (\text{B23})$$

where \mathcal{L} represents the Laplace transform operator. The Laplace transform of V_m is

$$\hat{V}_m(s) = \Gamma_m e^{-s\tau} \hat{z}_{-m}^{(1)}(s) + \hat{H}_m(s) = \frac{\hat{H}_m(s)}{\Lambda_m(s)}, \quad (\text{B24})$$

where we used (B11), (B12), and (B13). The Laplace transform $\hat{f}_m^{(1)}(\omega, s)$ is then from (B10)

$$\hat{f}_m^{(1)}(\omega, s) = -\frac{F_0(\omega)}{\omega - is/m} \frac{\hat{H}_m(s)}{\Lambda_m(s)}. \quad (\text{B25})$$

The Laplace transform of $V_m f_{n-m}^{(1)}$ is, from Appendix B3a,

$$\mathcal{L}[V_m f_{n-m}^{(1)}](s) = \frac{1}{2\pi i} \int_{\sigma_2 - i\infty}^{\sigma_2 + i\infty} \frac{\hat{H}_m(s')}{\Lambda_m(s')} \frac{F_0(\omega)}{\omega - i\frac{s-s'}{n-m}} \times \frac{\hat{H}_{n-m}(s-s')}{\Lambda_{n-m}(s-s')} ds'. \quad (\text{B26})$$

Remembering the note at the end of Appendix B3a and keeping in mind that we are interested in the asymptotic temporal evolution, we pick up the pole of $\hat{H}_m(s')$ which is at

$s' = -im\omega_{\text{ex}}$. The principal part of the Laplace transform is then

$$\text{PP}\mathcal{L}[V_m f_{n-m}^{(1)}](s) = \frac{\text{Res}(\hat{H}_m)}{\Lambda_m(-im\omega_{\text{ex}})} \frac{\hat{H}_{n-m}(s + im\omega_{\text{ex}})}{\Lambda_{n-m}(s + im\omega_{\text{ex}})} \frac{F_0(\omega)}{\omega - i\frac{s+im\omega_{\text{ex}}}{n-m}}, \quad (\text{B27})$$

where PP represents the part surviving in the limit $t \rightarrow \infty$, and $\text{Res}(\hat{H}_m) = \text{sgn}(m)ih_m/2$ is the residue of \hat{H}_m . Substituting the above expression into (B23), we have

$$\text{PP}\hat{z}_{-n}^{(2)}(s) = \frac{-1}{\Lambda_n(s)} \sum_m \frac{\text{Res}(\hat{H}_m)}{\Lambda_m(-im\omega_{\text{ex}})} \times \frac{\hat{H}_{n-m}(s + im\omega_{\text{ex}})}{\Lambda_{n-m}(s + im\omega_{\text{ex}})} T_{n,m}(s), \quad (\text{B28})$$

where

$$T_{n,m}(s) = \int_{\text{L}} \frac{g(\omega)}{(\omega - i\frac{s+im\omega_{\text{ex}}}{n-m})(\omega - i\frac{s}{n})} d\omega. \quad (\text{B29})$$

We pick up the pole of $\hat{H}_{n-m}(s + im\omega_{\text{ex}})$, which is at $s = -in\omega_{\text{ex}}$, for the asymptotic temporal evolution. Then,

$$e^{in\omega_{\text{ex}}t} \hat{z}_{-n}^{(2)}(t) \xrightarrow{t \rightarrow \infty} \frac{-1}{\Lambda_n(-in\omega_{\text{ex}})} \times \sum_m \frac{\text{Res}(\hat{H}_m) \text{Res}(\hat{H}_{n-m}) T_{n,m}(-in\omega_{\text{ex}})}{\Lambda_m(-im\omega_{\text{ex}}) \Lambda_{n-m}(-i(n-m)\omega_{\text{ex}})}. \quad (\text{B30})$$

We have to be careful for the value $T_{n,m}(-in\omega_{\text{ex}})$, because the integrand of $T_{n,m}(-in\omega_{\text{ex}})$ has the pole of order 2 at $\omega = \omega_{\text{ex}}$.

c. Nonlinear response coefficient

From now on, we focus on the nonlinear response of mode 2 induced by the external force of mode 1, i.e. $h_1 > 0$ and $h_l = 0$ ($l > 1$). Setting $n = 2$ and $m = 1$ in (B30), we have

$$e^{2i\omega_{\text{ex}}t} \hat{z}_{-2}^{(2)}(t) \xrightarrow{t \rightarrow \infty} \frac{T_{2,1}(-2i\omega_{\text{ex}})}{4\Lambda_2(-2i\omega_{\text{ex}})[\Lambda_1(-i\omega_{\text{ex}})]^2} h_1^2. \quad (\text{B31})$$

To obtain the value $T_{2,1}(-2i\omega_{\text{ex}})$, we first perform the partial fraction decomposition as

$$T_{2,1}(s) = \frac{2}{i(s + 2i\omega_{\text{ex}})} [I_1(s + i\omega_{\text{ex}}) - I_2(s)]. \quad (\text{B32})$$

In the limit $s \rightarrow -2i\omega'_{\text{ex}}$ ($\omega'_{\text{ex}} \neq \omega_{\text{ex}}$) from the upper-half s plane, we have

$$T_{2,1}(-2i\omega'_{\text{ex}}) = \frac{i}{\omega'_{\text{ex}} - \omega_{\text{ex}}} [\mathcal{G}^*(2\omega'_{\text{ex}} - \omega_{\text{ex}}) - \mathcal{G}^*(\omega'_{\text{ex}})]. \quad (\text{B33})$$

Further taking the limit $\omega'_{\text{ex}} \rightarrow \omega_{\text{ex}}$, we have

$$T_{2,1}(-2i\omega_{\text{ex}}) = i(\mathcal{G}^*)'(\omega_{\text{ex}}). \quad (\text{B34})$$

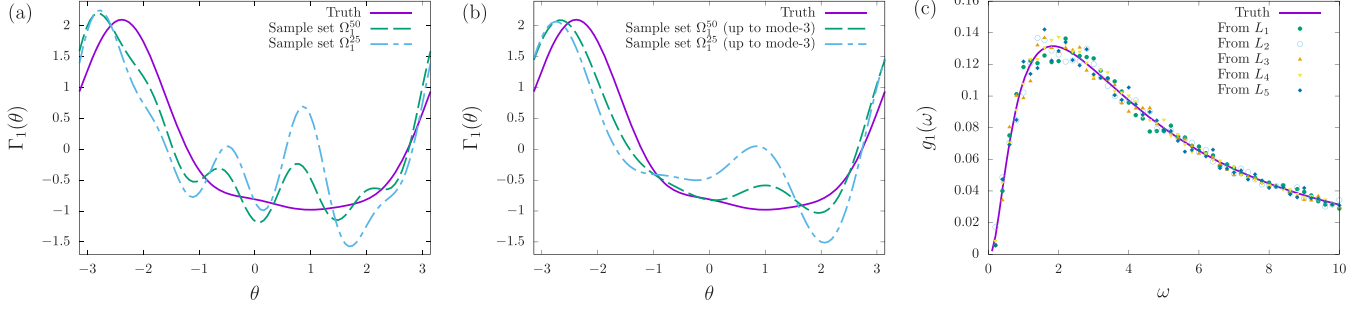


FIG. 5. Comparison between the truth and the inference in model 1 having $\tau > 0$. (a) The coupling function $\Gamma_1(\theta)$ is produced from the sample set Ω_1^{50} (green broken line) and Ω_1^{25} (blue chain line). (b) Same as (a) but the inferred $\Gamma_1(\theta)$ are truncated up to Fourier mode 3. (c) The natural frequency distribution $g_1(\omega)$ is obtained from the inferred L_1 (green filled circles), L_2 (blue open circles), L_3 (orange triangles), L_4 (yellow inverse triangles), and L_5 (dark-blue diamonds). The sample set is Ω_1^{50} .

The asymptotic temporal evolution of $z_2^{(2)}(t)$ is hence

$$e^{-2i\omega_{\text{ex}}t} z_2^{(2)}(t) \xrightarrow{t \rightarrow \infty} \chi_2^{11}(\omega_{\text{ex}}) h_1^2 + O(\|H\|^3), \quad (\text{B35})$$

where

$$\chi_2^{11}(\omega_{\text{ex}}) = \frac{i\mathcal{G}'(\omega_{\text{ex}})}{4\Lambda_2^*(-2i\omega_{\text{ex}})[\Lambda_1^*(-i\omega_{\text{ex}})]^2}. \quad (\text{B36})$$

Substituting

$$\begin{aligned} \Lambda_n(-i\omega_{\text{ex}}) &= \frac{1}{2}[2 - L_n^* \mathcal{G}^*(\omega_{\text{ex}})], \\ \Lambda_{-n}(i\omega_{\text{ex}}) &= \frac{1}{2}[2 - L_n \mathcal{G}(\omega_{\text{ex}})], \quad (n > 0) \end{aligned} \quad (\text{B37})$$

into the above expression, we have

$$\begin{aligned} \chi_2^{11}(\omega_{\text{ex}}) &= \frac{2i\mathcal{G}'(\omega_{\text{ex}})}{[2 - L_2(\omega_{\text{ex}})\mathcal{G}(\omega_{\text{ex}})][2 - L_1(\omega_{\text{ex}})\mathcal{G}(\omega_{\text{ex}})]^2} \\ &= \frac{2i\mathcal{G}'(\omega_{\text{ex}})}{[\mathcal{G}(\omega_{\text{ex}})]^3} \chi_2(\omega_{\text{ex}})[\chi_1(\omega_{\text{ex}})]^2, \end{aligned} \quad (\text{B38})$$

where we used (7).

APPENDIX C: INFERENCE OF L_1

The nonlinear response coefficient (B38) gives

$$\mathcal{G}'(\omega_{\text{ex}}) = \frac{\chi_2^{11}(\omega_{\text{ex}})[\mathcal{G}(\omega_{\text{ex}})]^3}{2i\chi_2(\omega_{\text{ex}})[\chi_1(\omega_{\text{ex}})]^2}. \quad (\text{C1})$$

We have another expression of $\mathcal{G}'(\omega_{\text{ex}})$. Solving (7) by $\mathcal{G}(\omega_{\text{ex}})$, we have

$$\mathcal{G}(\omega_{\text{ex}}) = \frac{2\chi_n(\omega_{\text{ex}})}{1 + L_n(\omega_{\text{ex}})\chi_n(\omega_{\text{ex}})}. \quad (\text{C2})$$

The derivation of (C2) gives

$$\begin{aligned} \mathcal{G}'(\omega_{\text{ex}}) &= 2 \frac{\chi_n'[1 + L_n\chi_n] - \chi_n[L_n\chi_n]'}{[1 + L_n\chi_n]^2} \\ &= \frac{\chi_n'(\omega_{\text{ex}}) + i\tau L_n[\chi_n(\omega_{\text{ex}})]^2}{2[\chi_n(\omega_{\text{ex}})]^2} [\mathcal{G}(\omega_{\text{ex}})]^2, \end{aligned} \quad (\text{C3})$$

where we used the definition $L_n = K_n e^{-i(\alpha_n + n\omega_{\text{ex}}\tau)}$. The combination between (C1) and (C3) provides for $n = 1$

$$\mathcal{G}(\omega_{\text{ex}}) = \frac{i\chi_2(\omega_{\text{ex}})[\chi_1'(\omega_{\text{ex}}) + i\tau L_1[\chi_1(\omega_{\text{ex}})]^2]}{\chi_2^{11}(\omega_{\text{ex}})}. \quad (\text{C4})$$

This expression and (C2) for $n = 1$ give the equality

$$\frac{1 + L_1(\omega_{\text{ex}})\chi_1(\omega_{\text{ex}})}{2\chi_1(\omega_{\text{ex}})} = \frac{\chi_2^{11}(\omega_{\text{ex}})}{i\chi_2(\omega_{\text{ex}})\{\chi_1'(\omega_{\text{ex}}) + i\tau L_1[\chi_1(\omega_{\text{ex}})]^2\}}. \quad (\text{C5})$$

This is the equation for determining L_1 .

1. For $\tau = 0$

In particular, L_1 is uniquely determined for $\tau = 0$ as

$$L_1 = K_1 e^{-i\alpha_1} = \frac{2\chi_2^{11}(\omega_{\text{ex}})}{i\chi_2(\omega_{\text{ex}})\chi_1'(\omega_{\text{ex}})} - \frac{1}{\chi_1(\omega_{\text{ex}})}. \quad (\text{C6})$$

2. For $\tau > 0$

We can infer L_1 from the quadratic equation (C5) for $\tau > 0$ as well as for $\tau = 0$. The quadratic equation is rewritten into

$$AL_1^2 + BL_1 + C = 0, \quad (\text{C7})$$

TABLE II. True and inferred parameter values of model 1 from (C9) and (C10), by taking the average over ω_{ex} . The time delay τ is inferred by procedure 1.

Model 1	τ	K_1	α_1	K_2	α_2	K_3	α_3	K_4	α_4	K_5	α_5
Truth	2	1.379	0.7884	0.568	-3.0316	0.154	-0.7546	0		0	
Ω_1^{50}	1.987	1.215	0.925	0.683	-2.663	0.257	0.694	0.119	2.108	0.289	0.991
Ω_1^{25}	1.995	0.857	0.806	0.956	-2.584	0.414	1.004	0.253	1.190	0.389	0.407

where

$$A(\omega_{\text{ex}}) = i\tau \frac{[\chi_1(\omega_{\text{ex}})]^2}{\chi_1'(\omega_{\text{ex}})}, \quad B(\omega_{\text{ex}}) = 1 + i\tau \frac{\chi_1(\omega_{\text{ex}})}{\chi_1'(\omega_{\text{ex}})},$$

$$C(\omega_{\text{ex}}) = \frac{1}{\chi_1(\omega_{\text{ex}})} - \frac{2\chi_2^{11}(\omega_{\text{ex}})}{i\chi_2(\omega_{\text{ex}})\chi_1'(\omega_{\text{ex}})}. \quad (\text{C8})$$

We have the two solutions to (C7), and we select the solution

$$L_1(\omega_{\text{ex}}) = -\frac{B(\omega_{\text{ex}})}{2A(\omega_{\text{ex}})} \left(1 - \sqrt{1 - \frac{4A(\omega_{\text{ex}})C(\omega_{\text{ex}})}{[B(\omega_{\text{ex}})]^2}} \right) \quad (\text{C9})$$

to have (C6) in the limit $\tau \rightarrow 0$, namely $A \rightarrow 0$. The inferred L_1 induces the other inferences of L_m through the relation

$$L_m(\omega_{\text{ex}}) - L_1(\omega_{\text{ex}}) = \frac{1}{\chi_1(\omega_{\text{ex}})} - \frac{1}{\chi_m(\omega_{\text{ex}})} \quad (m \geq 2). \quad (\text{C10})$$

The inferred parameter values are summarized in Table II for model 1. The inferred coupling function $\Gamma_1(\theta)$ and the natural frequency distribution $g_1(\omega)$ are compared with the true ones in Fig. 5. We observe rather large errors in higher order modes in $\Gamma_1(\theta)$, and precision is improved by truncating the Fourier series up to mode 3. Moreover, the errors tend to decrease as the number of samples increases, and $g_1(\omega)$ is well inferred irrespective of used modes.

-
- [1] A. T. Winfree, *The Geometry of Biological Time* (Springer, New York, 2001).
- [2] S. H. Strogatz, *Sync: How Order Emerges from Chaos in the Universe, Nature, and Daily Life* (Hyperion, New York, 2003).
- [3] A. Pikovsky, M. Rosenblum, and J. Kurths, *Synchronization: A Universal Concept in Nonlinear Sciences* (Cambridge University, Cambridge, England, 2001).
- [4] A. Palmigiano, T. Geisel, F. Wolf, and D. Battaglia, Flexible information routing by transient synchrony, *Nat. Neurosci.* **20**, 1014 (2017).
- [5] G. Buzsáki and E. I. Moser, Memory, navigation and theta rhythm in the hippocampal-entorhinal system, *Nat. Neurosci.* **16**, 130 (2013).
- [6] Y. Kuramoto, *Chemical Oscillations, Waves, and Turbulence* (Dover, New York, 2003).
- [7] H. Nakao, Phase reduction approach to synchronisation of nonlinear oscillators, *Contemp. Phys.* **57**, 188 (2016).
- [8] Y. Kuramoto and H. Nakao, On the concept of dynamical reduction: The case of coupled oscillators, *Phil. Trans. R. Soc. A* **377**, 20190041 (2019).
- [9] E. Tang and D. S. Bassett, Colloquium: Control of dynamics in brain networks, *Rev. Mod. Phys.* **90**, 031003 (2018).
- [10] R. F. Galán, G. B. Ermentrout, and N. N. Urban, Efficient estimation of phase-resetting curves in real neurons and its significance for neural-network modeling, *Phys. Rev. Lett.* **94**, 158101 (2005).
- [11] J. Miyazaki and S. Kinoshita, Determination of a coupling function in multicoupled oscillators, *Phys. Rev. Lett.* **96**, 194101 (2006).
- [12] I. T. Tokuda, S. Jain, I. Z. Kiss, and J. L. Hudson, Inferring phase equations from multivariate time series, *Phys. Rev. Lett.* **99**, 064101 (2007).
- [13] B. Kralemann, L. Cimponeriu, M. Rosenblum, A. Pikovsky, and R. Mrowka, Uncovering interaction of coupled oscillators from data, *Phys. Rev. E* **76**, 055201(R) (2007).
- [14] B. Kralemann, L. Cimponeriu, M. Rosenblum, A. Pikovsky, and R. Mrowka, Phase dynamics of coupled oscillators reconstructed from data, *Phys. Rev. E* **77**, 066205 (2008).
- [15] W. D. Penny, V. Litvak, L. Fuentemilla, E. Duzel, and K. Friston, Dynamic causal models for phase coupling, *J. Neurosci. Methods* **183**, 19 (2009).
- [16] T. Stankovski, A. Duggento, P. V. E. McClintock, and A. Stefanovska, Inference of time-evolving coupled dynamical systems in the presence of noise, *Phys. Rev. Lett.* **109**, 024101 (2012).
- [17] K. Ota and T. Aoyagi, Direct extraction of phase dynamics from fluctuating rhythmic data based on a Bayesian approach, [arXiv:1405.4126](https://arxiv.org/abs/1405.4126).
- [18] A. Pikovsky, Reconstruction of a random phase dynamics network from observations, *Phys. Lett. A* **382**, 147 (2018).
- [19] F. Mori and H. Kori, Noninvasive inference methods for interaction and noise intensities of coupled oscillators using only spike time data, *Proc. Natl. Acad. Sci. USA* **119**, e2113620119 (2022).
- [20] L. Paninski, J. W. Pillow, and E. P. Simoncelli, Maximum likelihood estimation of a stochastic integrate-and-fire neural encoding model, *Neural Comput.* **16**, 2533 (2004).
- [21] Y. Roudi and J. Hertz, Mean field theory for nonequilibrium network reconstruction, *Phys. Rev. Lett.* **106**, 048702 (2011).
- [22] Y. Terada, T. Obuchi, T. Isomura, and Y. Kabashima, Objective and efficient inference for couplings in neuronal networks, *Adv. Neural Inf. Proc. Sys.* **31**, 4971 (2018).
- [23] B. Bravi and P. Sollich, Inference for dynamics of continuous variables: The extended Plefka expansion with hidden nodes, *J. Stat. Mech.* (2017) 063404.
- [24] M. K. S. Yeung and S. H. Strogatz, Time delay in the Kuramoto model of coupled oscillators, *Phys. Rev. Lett.* **82**, 648 (1999).
- [25] E. Montbrió, D. Pazó, and J. Schmidt, Time delay in the Kuramoto model with bimodal frequency distribution, *Phys. Rev. E* **74**, 056201 (2006).
- [26] H. Sakaguchi, Cooperative phenomena in coupled oscillator systems under external fields, *Prog. Theor. Phys.* **79**, 39 (1988).
- [27] H. Daido, Susceptibility of large populations of coupled oscillators, *Phys. Rev. E* **91**, 012925 (2015).
- [28] Y. Terada and Y. Y. Yamaguchi, Linear response theory for coupled phase oscillators with general coupling functions, *J. Phys. A* **53**, 044001 (2020).
- [29] For example, transcranial magnetic stimulation may realize a situation where the brain systems are perturbed without high invasiveness [30].
- [30] M. C. Ridding and J. C. Rothwell, Is there a future for therapeutic use of transcranial magnetic stimulation? *Nat. Rev. Neurosci.* **8**, 559 (2007).
- [31] D. J. Watts and S. H. Strogatz, Collective dynamics of “small-world” networks, *Nature (London)* **393**, 440 (1998).

- [32] H. Hong, M. Y. Choi, and B. J. Kim, Synchronization on small-world networks, *Phys. Rev. E* **65**, 026139 (2002).
- [33] R. Yoneda, K. Harada, and Y. Y. Yamaguchi, Critical exponents in coupled phase-oscillator models on small-world networks, *Phys. Rev. E* **102**, 062212 (2020).
- [34] T. Ichinomiya, Frequency synchronization in a random oscillator network, *Phys. Rev. E* **70**, 026116 (2004).
- [35] H. Daido, Population dynamics of randomly interacting self-oscillators. I: Tractable models without frustration, *Prog. Theor. Phys.* **77**, 622 (1987).
- [36] S. Gupta, M. Potters, and S. Ruffo, One-dimensional lattice of oscillators coupled through power-law interactions: Continuum limit and dynamics of spatial Fourier modes, *Phys. Rev. E* **85**, 066201 (2012).
- [37] H. Chiba and G. S. Medvedev, The mean field analysis of the Kuramoto model of graphs I. The mean field equation and transition point formulas, *Discrete Contin. Dyn. Syst.* **39**, 131 (2019).
- [38] H. Chiba and G. S. Medvedev, The mean field analysis of the Kuramoto model of graphs II. Asymptotic stability of the incoherent state, center manifold reduction, and bifurcations, *Discrete Contin. Dyn. Syst.* **39**, 3897 (2019).
- [39] H. Chiba, G. S. Medvedev, and M. S. Mizuhara, Bifurcations in the Kuramoto model on graphs, *Chaos* **28**, 073109 (2018).
- [40] J. M. Palva, S. Monto, S. Kulashekhar, and S. Palva, Neuronal synchrony reveals working memory networks and predicts individual memory capacity, *Proc. Natl. Acad. Sci. USA* **107**, 7580 (2010).
- [41] S. Ostojic, Two types of asynchronous activity in networks of excitatory and inhibitory spiking neurons, *Nat. Neurosci.* **17**, 594 (2014).
- [42] J. Li and W. L. Shew, Tuning network dynamics from criticality to an asynchronous state, *PLoS Comput. Biol.* **16**, e1008268 (2020).
- [43] S. H. Strogatz, R. E. Mirollo, and P. C. Matthews, Coupled nonlinear oscillators below the synchronization threshold: Relaxation by generalized Landau damping, *Phys. Rev. Lett.* **68**, 2730 (1992).
- [44] F. C. Hoppensteadt and E. M. Izhikevich, *Weakly Connected Neural Networks* (Springer, New York, 1997).
- [45] H. Daido, Order function and macroscopic mutual entrainment in uniformly coupled limit-cycle oscillators, *Prog. Theor. Phys.* **88**, 1213 (1992).
- [46] C. Lancellotti, On the Vlasov limit for systems of nonlinearly coupled oscillators without noise, *Transp. Theory Stat. Phys.* **34**, 523 (2005).
- [47] D. Hansel, G. Mato, and C. Meunier, Phase dynamics for weakly coupled Hodgkin-Huxley neurons, *Europhys. Lett.* **23**, 367 (1993).
- [48] D. Hansel, G. Mato, and C. Meunier, Synchrony in excitatory neural networks, *Neural Comput.* **7**, 307 (1995).
- [49] E. M. Izhikevich, Polychronization: Computation with spikes, *Neural Comput.* **18**, 245 (2006).
- [50] G. Buzsáki and K. Mizuseki, The log-dynamic brain: How skewed distributions affect network operations, *Nat. Rev. Neurosci.* **15**, 264 (2014).
- [51] H. Sakaguchi and Y. Kuramoto, A soluble active rotator model showing phase transitions via mutual entertainment, *Prog. Theor. Phys.* **76**, 576 (1986).
- [52] J. O'Byrne and K. Jerbi, How critical is brain criticality? *Trends Neurosci.* **45**, 820 (2022).
- [53] D. Barson, A. S. Hamodi, X. Shen, G. Lur, R. T. Constable, J. A. Cardin, M. C. Crair, and M. J. Higley, Simultaneous mesoscopic and two-photon imaging of neuronal activity in cortical circuits, *Nat. Methods* **17**, 107 (2020).
- [54] G. Arnulfo, S. H. Wang, V. Myrov, B. Toselli, J. Hirvonen, M. M. Fato, L. Nobili, F. Cardinale, A. Rubino, A. Zhigalov, S. Palva, and J. M. Palva, Long-range phase synchronization of high-frequency oscillations in human cortex, *Nat. Commun.* **11**, 5363 (2020).
- [55] V. Lucarini, G. A. Pavliotis, and N. Zagli, Response theory and phase transitions for the thermodynamic limit of interacting identical systems, *Proc. R. Soc. A* **476**, 20200688 (2020).
- [56] K. Kotani, I. Yamaguchi, Y. Ogawa, Y. Jimbo, H. Nakao, and G. B. Ermentrout, Adjoint method provides phase response functions for delay-induced oscillators, *Phys. Rev. Lett.* **109**, 044101 (2012).
- [57] V. Novičenko and K. Pyragas, Phase reduction of weakly perturbed limit cycle oscillators in time-delay systems, *Physica D* **241**, 1090 (2012).